Response of a Prototype Brain Material Subjected to Rotational Acceleration

회전가속에 대한 프로토타입 뇌재료의 반응

E. S. Lee*, S. Im**
이 응 선, 임 세 영

ABSTRACT

With the objective of studying the response of brain tissue in a transient rotational acceleration of the head, as occurs in car crash, the problem of a cylindrical case containing a prototype brain material of silicone gel and subjected to a rotational acceleration around the axis of the cylinder is analysed. The prototype material is considered to be homogeneous and isotropic, and is modeled alternatively as a linear elastic or a linear viscoelastic solid.

The computational model for the present problem consists of a 3-dimensional isoparametric finite element model, wherein large deformations and large strains are treated through the updated Lagrangian approach. A comparison of the results of the present 3-dimensional computations, with the attendant assumptions on material data, is made with the results of independent experimental study. The deformation profiles and the major characteristics of response of the brain material are in good agreement with the test results. Moreover, the study suggests the possibility that the use of more accurate material data may yield very useful results even appropriate for accurate quantification of deformations.

1. Introduction

When mechanical loads are applied to the head, the deformation, strains or stress within the brain can exceed the tolerance limit, resulting in a head injury. Therefore, it is necessary to better understand the biomechanical aspects of head injury under certain specific kinematic conditions and loading. A number of experimental, analytical, and numerical studies have been carried out on the subject of brain damage under a transient dynamic loading of the head.

Stritch pointed out that the high shear strain may damage tissues in the cortical and subcortical regions of the brain tissue; the translational component of the impact was considered to be non-injurious [1]. Experi-

* 미국 조오지아 공과대학 계산역학센터
** 정회원, 한국과학기술원 기계공학과

ments have been conducted by Ommaya [2] in 3 sub-human primate species, and he was able to confirm that the rotational excitation of a short duration may produce cerebral concussion. Engine and Wang [3] studied analytically the steady state response of a solid sphere of an elastic material, under a radial harmonic excitation, and discussed the concept of a complex dynamic shear modulus. Wang [4] studied analytically the response of brain which is modeled as a linear isotropic viscoelastic solid constrained by a rigid skull. Other examples of works based upon viscoelastic constitutive model include Lung [5] and Misra [8]. Merchant and Crispino [6] modeled the head as a fluid-filled spherical shell, or alternatively as a prolate ellipsoid of revolution.

Recently Thibault and his associates at the University of Pennsylvania [9, 10] carried out an experiment to find the transient response in the brain-skull system subjected to translational or rotational acceleration. A cylinder that contains the silicone gel for the surrogate brain tissue was used to model the brain-skull system in the test. The test captures well the high shear strains, which are known to be critical to brain injury near the skull-tissue boundary under rotational acceleration transient[1]. It is, however, extremely difficult to quantify the deformation field accurately from such a test.

The current state of the science of computational mechanics renders numerical simulation of a head injury to be an alternative to an experiment. The purpose of the present work is to perform numerical simulation of the test conducted at the University of Pennsylvania; this will make possible comparison of the deformation profile between the test and the numerical simulation, and from this the possibility is examined that the numerical simulation may provide a proper quantification of the deformation field so that it can substitute for the expensive test. For this a three dimensional finite element model, wherein a linear elastic or a linear viscoelastic material is assumed for the surrogate brain tissue, is employed to analyse the transient response of the brain material under rotational acceleration. The computational model comprises 8-node isoparametric elements, and large deformations including finite strain cases are treated through the update Lagrangian approach. The data computed at node points in the finite element grids are interpolated or extrapolated through a smooth function interpolation technique onto a grid that was used in the test by Thibault and his associates.

A comparison of the results of the present 3-dimensional computations, with the attendant assumptions on material data, is made with the test results by Thibault and his associates [9, 10]. These comparisons of the deformation profiles are quite encouraging. The phenomenon of large shear strains near the periphery of the cylindrical case, in the prototype material, under intense rotational acceleration is captured well in the computations. The core region experiencing rigid body motion is also predicted well in the simulation, and the time lag between the displacement of the silicone gel and the input displacement is in good agreement with the test result.

2. Statement of the problem

At the instant of car crash, a driver's head experiences a rotational transient motion about the neck and is subjected to a severe rotational acceleration, which results in the damage to the brain tissue near the cortical

and subcortical region due to high shear deformation. For better understanding of the biomechanical aspects of the head injury under such circumstances, Thibault and his associates [9, 10] at the University of Pennsylvania devised an experimental apparatus, as shown in Fig. 1, to simulate such a loading and kinematic condition. They employed a cylindrical steel case containing silicone gel to simulate the skull-brain system (see Fig. 2). This container was subjected to the intense rotational transient that the driver's head would experience in car crash, as shown in Fig. 1 wherein the distance between the center of mass (CM) and the center of rotation (CR) is adjustable. Because of the dominant effect of the rotational acceleration upon the brain damage, the case of purely rotational acceleration (CM=CR) was under intensive study. Uniform square grids were made on the silicone gel before experiment, and a high speed camera was used to capture the deformed grid profiles during acceleration transient. The load curve measured under the purely rotational acceleration is shown in Fig. 4 in terms of acceleration and displacement. The maximum displaced angle is about 65 degree as shown in Fig. 1.

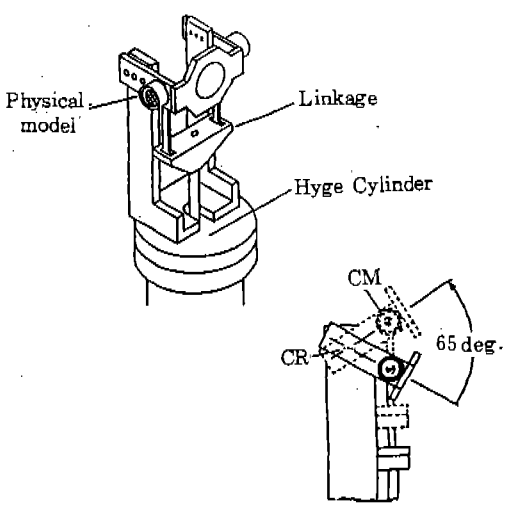

Fig. 1 Experimental apparatus used by Thibault [10].

For numerical simulation of this experiment, we perform three dimensional finite element analysis for the cylindrical brain-skull model, as shown in Fig. 2, wherein S_u and S_t denote surface segments where displacement and traction boundary conditions are prescribed, respectively. The top of the container is traction free while the lateral and bottom surfaces undergo prescribed displacements due to rotational acceleration. It means that no slip occurs between the prototype brain material and the case except at the top portion of the brain-skull model.

3. Basic Equations and Solution Procedures

3.1. Constitutive Equations

Several authors, such as Merchant and Crispino [6], and Akkas [7], employed a fluid-filled container model for skull-brain system. According to the experiment conducted by Thibault and has associates [9, 10], however, it is more appropriate to assume the brain tissue to be an elastic solid rather than a fluid; for the surrogate brain tissue almost recovers its initial configuration long after the transient loading. To be precise, most biological materials will display viscoelastic properties which include nonlinearity due to time dependence. In addition to an elastic model therefore a linear viscoelastic constitutive model is employed, which is now to be discussed.

For small linear viscoelastic deformations, the constitutive equation may be written as

$$\underset{\sim}{\sigma}' = 2\int_0^t R(t-\tau)\frac{d\underset{\sim}{e}'}{d\tau}\,d\tau \quad \text{and} \quad \mathrm{tr}\,\underset{\sim}{\sigma} = 3k\,\mathrm{tr}\,\underset{\sim}{e} \tag{1.a,b}$$

which represent the viscoelastic behavior of the deviatoric part and the purely elastic behavior of the volumetric part; here $\underset{\sim}{\sigma}'$, $\underset{\sim}{e}'$ are the deviatoric parts of the Cauchy stresses and the infinitesimal strains, and R(t), k are the shear relaxation function and bulk modulus, respectively. For extension of this constitutive model to finite strain deformations, we introduce the rotated Cauchy stress $\bar{\sigma}$ and the rotated rate of deformation $\bar{D}$,

$$\bar{\underset{\sim}{\sigma}} = \underset{\sim}{R}^{T} \cdot \underset{\sim}{\sigma} \cdot \underset{\sim}{R} \quad , \quad \bar{\underset{\sim}{D}} = \underset{\sim}{R}^{T} \cdot \underset{\sim}{D} \cdot \underset{\sim}{R} ,$$

where $\underset{\sim}{R}$ is the rotation tensor in the polar decomposition of the deformation gradient and $\underset{\sim}{D}$ is the rate of deformation tensor. For generalization of equation(1.a) to the case of large deformation, noting that $\bar{\underset{\sim}{\sigma}}$ and $\bar{\underset{\sim}{D}}$ are both referred to the undeformed configuration, we may consider,

$$\bar{\underset{\sim}{\sigma}}' = 2\int_0^t R(t-\tau)\,\bar{\underset{\sim}{D}}'\,d\tau ,$$
$$\mathrm{tr}\,\dot{\underset{\sim}{\sigma}} = 3k\,\mathrm{tr}\,\underset{\sim}{D} \qquad (2.a,b)$$

Such a generalization of the contitutive equations from infinitesimal deformations to large deformations is not unique; we may generalize equations (1.a,b) using the 2-nd Piola Kirchhoff stress and the Green strain rate, which leads to an apparent difficulty, however, in decomposing the deformation increments into the deviatoric part and the volumetric part for finite strain deformation. The constitutive model (2.a,b) enables us to avoid such a difficulty when deformations become large. In the present study, we use the following function for the relaxation function,

$$R(t) = G_2 + (G_1 - G_2)\,e^{-\alpha t} \qquad (3)$$

where G_1 and G_2 are the initial and the final shear modulus, respectively, or alternatively they will be called the short time and the long time shear modulus. The mechanical analogy of this viscoelastic model is shown schematically in Fig.5. The relationship between this mechanical model and the relaxation model (1) is given as

$$G_2 = K \ , \ G_1 = K_1 + K, \ \alpha = K_1/C \qquad (4)$$

Differentiating Eq.(1.a) or from the mechanical model, Fig. 5, we can obtain the following differential form

$$\bar{\underset{\sim}{\sigma}}' + \frac{1}{\alpha}\frac{d\bar{\underset{\sim}{\sigma}}'}{dt} = 2\left(G_2\,\gamma + \frac{G_1}{\alpha}\bar{\underset{\sim}{D}}'\right) ,$$
$$\gamma = \int_0^t \bar{\underset{\sim}{D}}'(\tau)\,d\tau \qquad (5)$$

From this equation, it follows that the complex shear modulus-like-parameter $\bar{G}$, which corresponds to $\bar{\sigma}_{ij}'/(2\gamma_{ij})$, in terms of sinusoidal input frequency ω is given as

$$\bar{G}(i\omega) = \frac{\alpha^2 G_2 + \omega^2 G_1}{\alpha^2 + \omega^2} + \frac{(G_1 - G_2)\,\alpha\omega}{\alpha^2 + \omega^2}\,i \qquad (6)$$

We also employ the linear elastic constitutive equation of isotropic materials in terms of the rotated stress and the rate of deformations,

$$\dot{\bar{\underset{\sim}{\sigma}}}' = 2G\bar{\underset{\sim}{D}}' \quad \text{and} \quad \mathrm{tr}\,\dot{\underset{\sim}{\sigma}} = 3k\,\mathrm{tr}\,\underset{\sim}{D} \qquad (7.a,b)$$

where G is the shear modulus. Note that this equation is reduced to Hooke's law for infinitesimal deformations, and that it is obtained as a limiting case of equation (2.a,b) by taking $G_1 = G_2$.

The aforementioned models may not thoroughly describe the characteristics of the real brain material, but serve as simple models, which are taken to be enough for the present primitive skull-brain model. Moreover, equation (7.a,b) does not represent the strict hyperelastic behavior for large deformations, as

pointed out by Simo and Pister[13]; however, it does not show any unacceptable response at the strain level less than 100%.

3.2. Finite Element Formulation

We use the updated Lagrangian displacement F.E.M. to obtain the transient response of the aforementioned skull-brain system. The governing equations and the boundary conditions for F.E.M. formulation are summarized as

linear momentum balance in the absense of a body force:

$$\frac{\partial T_{ij}}{\partial x_i} = \rho \ddot{x}_j \tag{8}$$

angular momentum balance:

$$F_{ij}T_{jk} = F_{kj}T_{jl} \tag{9}$$

traction boundary conditions:

$$T_{ij}n_i = \bar{t} \quad \text{on} \quad S_{tj} \tag{10}$$

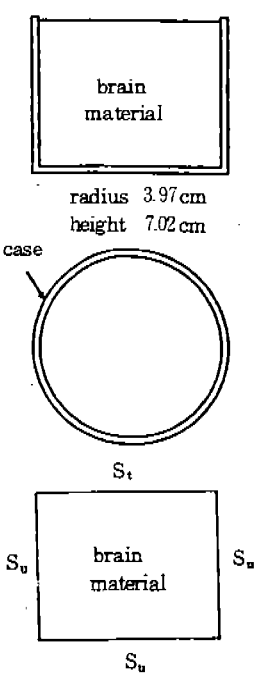

Fig. 2 Brain-skull model.

displacement boundary conditions:

$$u_j = \bar{u}_j \quad \text{on} \quad S_{uj} \tag{11}$$

where

- F_{ij} : defomation gradient
- T_{ij} : nominal stress tensor
- u_j : displacement
- t_i : traction
- S_{tj} : part of the body boundary on which t_j is prescribed
- S_{uj} : part of the body boundary on which u_j is prescribed

Here the angular momentum balance (9) is nothing but the symmetry requirement for the Cauchy stress, and it is satisfied identically when the constitutive equation is prescribed in terms of the rotated or the Cauchy stress as given in equations (2.a,b) and (7.a,b). Suppose successive configurations corresponding to time $t = t_0, t_1, t_2, \ldots t_N \ldots . t_f$, and we denote this sequence of configurations by $\Omega^1, \Omega^2, \Omega^3, \ldots \Omega^N, \Omega^{N+1}, \ldots . \Omega^f$. In the updated Lagrangian formulation, the most recent configuration among those which we have obtained is taken for the reference configuration to solve for the subsequent configuration under the corresponding external load increment.

As a start toward the formulation, suppose we have obtained all the configurations up to Ω^N. To obtain the solution for the next configuration Ω^{N+1}, we write the weak form of the linear momentum balance and the traction boundary condition for Ω^{N+1} with Ω^N being taken as the reference configuration.

$$\int_{\Omega^N} \omega_j \frac{\partial T^N_{ij}}{\partial x^N_i} dV + \int_{\Omega^N} \omega_j \frac{\partial \Delta T_{ij}}{\partial x^N_i} dV - \int_{\Omega^N} \omega_j \rho \ddot{x}^{N+1}_j dV + \int_{S_{tj}} \bar{\omega}_j (T^N_{ij} n_i + \Delta T_{ij} n_i - \bar{t}^{N+1}_j) dS = 0 \tag{12}$$

Here $\bar{\omega}_j$ and ω_j are the weight functions and we have taken

$$\omega_j = -\bar{\omega}_j \text{ on } S_{tj}, \text{ and } \omega_j = 0 \text{ on } S_{uj},$$

and we have used

$$T_{ij}^{N+1} = T_{ij}^{N} + \Delta T_{ij} \tag{13}$$

Integrating equation (12) by parts and applying the divergence theorem with the aid of equation(13), we reach the following form,

$$\int_{\Omega^N} \Delta T_{ij} \frac{\partial \omega_j}{\partial x_i^N} dV = \int_{S_{tj}} \bar{t}_j^{N+1} \omega_j \, dS - \int_{\Omega^N} T_{ij}^N \frac{\partial \omega_j}{\partial x_i^N} dV + \int_{\Omega^N} \rho \ddot{x}_j^{N+1} \omega_j dV \tag{14}$$

Expressing the nominal stress increment ΔT_{ij} in terms of the increment of the 2-nd Piola-Kirchhoff stress ΔS_{ij} and the displacement increment Δu_i, we rewrite the above as

$$\int_{\Omega^N} (\Delta S_{ij} + \sigma_{im} \frac{\partial \Delta u_j}{\partial x_m^N}) \frac{\partial \omega_j}{\partial x_i^N} dV = \int_{St_j} \bar{t}^{N+1} \omega_j dS - \int_{\Omega^N} T_{ij}^N \frac{\partial \omega_j}{\partial x_i^N} dV + \int_{\Omega^N} \rho \ddot{x}_j^{N+1} \omega_j dV \tag{15}$$

Note that the nominal stress and the 2-nd Piola-Kirchhoff stress appearing above are all referred to the configuration Ω^N, not to the undeformed configuration. The two terms on the left hand side of equation (15) yield the stiffness due to the incremental stress and the initial stress, respectively; on the other hand, the three terms on the right hand side give the external load, the internal force and the inertia force, respectively. Noting that the constitutive equation (2.a) is given in terms of the rotated Cauchy stress, we rewrite the first term on the left hand side in terms of the Green-Nagdhi increment

$$\Delta S_{ij} = \Delta \sigma_{ij}^{GR} - \left[\left(\frac{\partial \Delta u_i}{\partial x_m^N} - \Delta R_{ik} R_{mk} \right) \sigma_{mj} - \sigma_{im} \left(\frac{\partial \Delta u_j}{\partial x_m^N} + \Delta R_{mk} R_{jk} \right) + \sigma_{ij} \Delta \epsilon_{kk} \right] \tag{16}$$

where

$$\Delta \sigma_{ij}^{GR} = R_{im} \Delta \bar{\sigma}_{mn} R_{jn}, \quad \Delta \epsilon_{ij} = \frac{1}{2} \left(\frac{\partial \Delta u_i}{\partial x_j^N} + \frac{\partial \Delta u_j}{\partial x_i^N} \right) \cong D_{ij} \Delta t \tag{17.a,b}$$

A proper manipulation of equation (2.a,b) gives the following form of an approximate incremental relation.

$$\Delta \sigma_{ij}^{GR} = C_{ijk\ell} \Delta \epsilon_{k\ell} \tag{18}$$

where C_{ijkl} is the incremental viscoelastic stiffness, given in Appendix. This is now used to represent $\Delta \sigma_{ij}^{GR}$ in the displacement increment Δu_i through (17.b). For accurate computation of stiffness, all the remaining terms inside the bracket of equation (16) need to be considered. This, however, would entail very complex algebra and would involve a great deal of numerical computation. For stiffness computation, we therefore neglect all terms other than the first term in equation (16) and the second term on the right hand side of equation (15). Fast convergence of the Newton type scheme is sacrificed due to this; but this will not affect the accuracy of the solution whenever iteration reaches convergence, as long as the constitutive equation (2.a,b) is properly implemented in the stress update

procedure so that the unbalanced force on the right hand side of equation (15) can be accurately calculated. Numerically the use of an approximate stiffness, with some terms neglected, is equivalent to using the modified Newton's method in solving nonlinear equations.

For symmetric stiffness we take $\omega_i = \delta\Delta u_i$ in equations (15) and (16), and taking the straightforward F.E. formulation after introducing an appropriate shape function, we finally obtain the following incremental equation,

$$K_{IJ}^{N}\,\Delta\phi_J = P_I^{N+1} - F_I^{N} + M_{IJ}\,\ddot{\phi}_J^{N+1} \quad (19)$$

where $P_I^{N+1} = P_I^N + \Delta P_I$ is the external load at $t=t^{N+1}$, F_I^N the internal force vector, K^N_{IJ} and M_{IJ} are the tangent stiffness and mass matrix, and $\phi_J^{N+1}=\phi_J^N+\Delta\phi_J$ is the nodal degree of freedom. For simplicity we use the lumped mass matrix, which remains constant throughout analysis, and therefore does not need updating every time step. For accurate calculation of the stress divergence or the internal force term F_I^N, the constitutive equation (2.a,b) should be properly implemented in the stress update procedure. We here use the scheme proposed by Key [12]. For time integration, we use the Newmark method, which becomes an unconditionally stable implicit scheme with a proper choice of the Newmark constants. Application of the Newmark scheme to equation (19) leads to the following form suitable for iteration (see the reference [14] for details),

$$\hat{K}_{IJ}^{(N,i-1)}\,\Delta\phi_J^{(N,i)} = P_I^{N+1} - \hat{F}_I^{(N,i-1)} \quad (20)$$

where

$$\hat{K}_{IJ}^{(N,i-1)} = K_{IJ}^{(N,i-1)} + \frac{1}{\beta\Delta t^2} M_{IJ} \quad (21.a)$$

$$\hat{F}_I^{(N,i-1)} = F_I^{(N,i-1)} + \frac{1}{\beta\Delta t^2} M_{IJ}(\phi_J^{(N,i-1)} - \phi_J^{(N)}) - \frac{1}{\beta\Delta t} M_{IJ}\dot{\phi}_J^{(N)} - (\frac{1}{2\beta} - 1)M_{IJ}\ddot{\phi}_J^{(N)} \quad (21.b)$$

$$\ddot{\phi}_J^{(N,i)} = \frac{1}{\beta\Delta t^2}\left\{\phi_J^{(N,i)} - \phi_J^{(N)}\right\} - \frac{\dot{\phi}_J^{(N)}}{\beta\Delta t} - (\frac{1}{2\beta} - 1)\,\ddot{\phi}_J^{(N)} \quad (21.c)$$

$$\dot{\phi}_J^{(N,i)} = \dot{\phi}_J^{(N)} + \Delta t(1-\gamma)\ddot{\phi}_J^{(N)} + \gamma\Delta t\,\ddot{\phi}_J^{(N,i)} \quad (21.d)$$

where β,γ are the Newmark constants. Here the superscript (N, i) indicates the i-th iteration at the time step N, and the incremental degree of freedom $\Delta\phi_J^{(N,i)}$ is related to $\phi_J^{(N,i)}$ as

$$\phi_J^{(N,i)} = \phi_J^{(N,i-1)} + \Delta\phi_J^{(N,i)} = \phi_J^{(N)} + \sum_{k=1}^{i}\Delta\phi_J^{(N,k)} \quad (22)$$

where $\phi_J^{(N,i)}$ converges to $\phi_J^{(N+1)}$ as i increases sufficiently. Note that the velocity and the acceleration are given by equations (21.c) and (21.d), respectively, once the incremental displacement $\Delta\phi_J^{(N,i)}$ is obtained from equation (20), and subsequently $\phi_J^{(N,i)}$ from equation (22).

4. Numerical Results and Discussion

The three dimensional finite element modelling of the eight node isoparametric elements is used for the present analysis (so that it can be used for analysis of nonaxisymmetric motion later). The mesh configuration

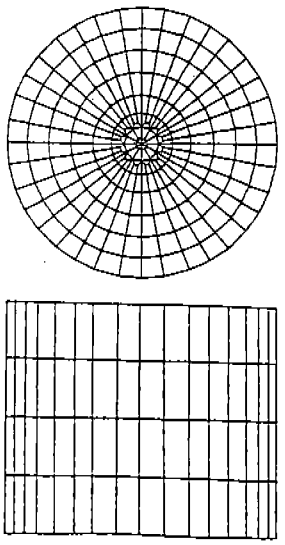

Fig. 3 The three dimensional finite element mesh discretization for the brain material.

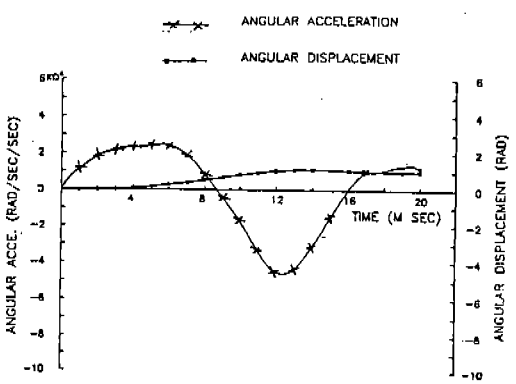

Fig. 4 Load curves (acceleration and displacement of the container) in the rotational transient.

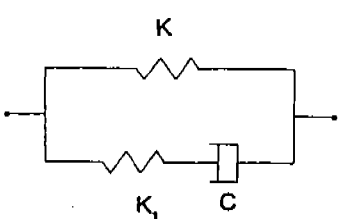

Fig. 5 Mechanical model for the standard linear solid.

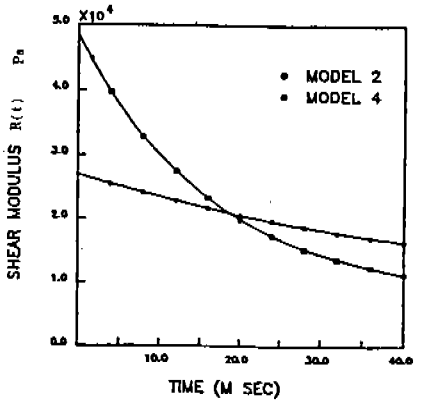

Fig. 6 Relaxation functions for the viscoelastic models.

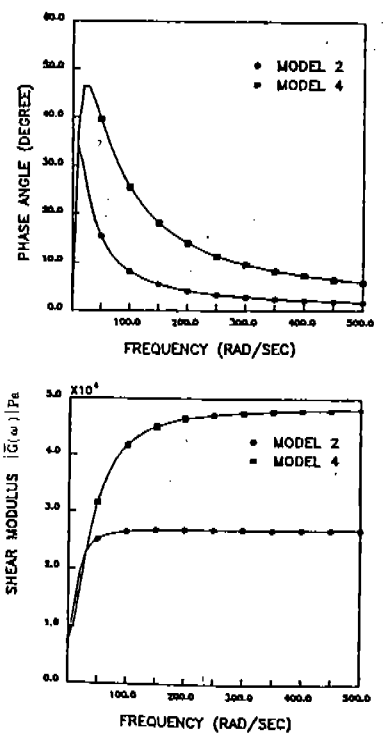

Fig. 7 Frequency characteristics of the viscoelastic modes.

is shown in Fig. 3, and the other configurations in Fig. 8 are introduced to examine the sensitivity of solution to the mesh configuration. The physical dimension and the density of the

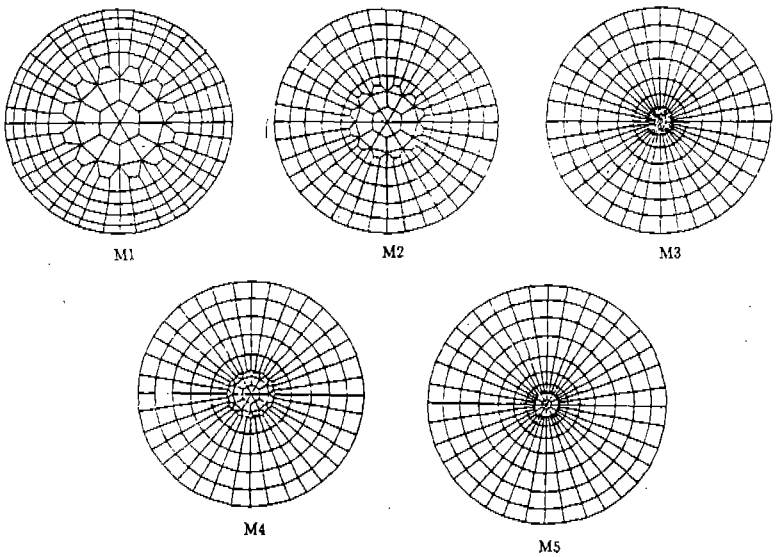

Fig. 8 Mesh configurations

silicone gel are given as

height : 7.02 cm
radius : 3.97 cm
density: 0.95 gm/cm^3

The elastic and viscoelastic properties of the silicone gel are not easy to determine accurately; according to the test results [10] there are some variations even in Young's modulus. The following four material models are used for numerical simulation:

model 1 (elastic)	Shear modulus G: 2.69 x 10^{4}Pa
	Poisson's ratio ν : 0.49
model 2 (viscoelastic)	G_1 : 2.69 x 10^4 Pa
	G_2 : 7.54 x 10^3 Pa
	k : 1.25 x 10^6 Pa
	α : 601/sec
model 3 (elastic)	G : 4.84 x 10^4 Pa
	ν : 0.49
model 4 (viscoelastic)	G_1 : 4.84 x 10^4 Pa
	G_2 : 7.54 x 10^3 Pa
	k : 2.25 x 10^6 Pa
	α : 201/sec

Poisson's ratio ν=0.49, close to 0.5, implies that the material is almost incompressible. The long time shear modulus G_2 is determined from the relation $G_2 = E/(2 + 2\nu)$ and from Young's modulus of the reference [10] (E= 2.246 x 10^4 Pa, C1, B200), which was obtained from the static test. There are, however, no available data for G_1, k and α, and these are therefore conjectured. It is noticed that the shear modulus G of model 1 is equal to the short time shear modulus G_1 of model 2, and that the shear modulus of model 3 to the short time modulus of model 4. The relaxation functions and the frequency characteristics are shown in Fig.6 and in Fig.7. Fig.7 shows that the shear modulus change on the frequency domain is negligible when the frequency is higher than 150 rad/sec.

The time dependent displacement boundary conditions, appearing in Fig.4, are imposed on the displacement boundary S_u of Fig.2 The Newmark constants are taken as β=0.45, and γ=0.75, which assure the unconditional stability. For the time step size, we use Δt =

2.5×10^{-4} sec. The effect of time step size is found to be negligible when Δt is smaller than 5×10^{-4} sec.

In the beginning, we use the mesh configuration M1, which has very coarse mesh in the central region (Fig.8). The use of this mesh, might be justified because it is expected that shear distortion will be very small in the central region and therefore only little error will occur. However, the results show that the coarse mesh in the central region gives rise to a spurious response as time exceeds 16 m sec. This has been rectified gradually as the region of coarse mesh shrinks in the center along with the mesh configurations M2, M4, M5, and M3. The three mesh configurations M4, M5, M3 turns out to give virtually the same results.

The output nodal displacements are interpolated to give the deformed configuration of the square grid used in the experiment, so that a comparison may be made of the deformed configurations between the numerical simulation and the test. Because of the limitation of space available, the results only for the material models 1 and 2, which turn out to produce better results than the models 3 and 4 are shown in Fig.9 and 10, where the deformed shapes from the test are shown on the top. The shear strain component A_{r_θ} of the Almansi strain tensor [11] is also plotted below the deformed shape. The numerical results for deformation profiles are seen to be very similar to the test results obtained by Thibault [10]. The numerical results agree with the experimental results in that the displacement of the brain material lags behind the input rotational displacement during the acceleration phase. Under the deceleration, the inner region of the brain model continues to rotate, overshooting the outer input displacement up to the time of 10 m sec. There is found the undeformed core exhibiting rigid body motion as in the experiment. The large shear strain near the periphery of the cylindrical case is also captured well in the numerical simulation.

From Fig.9 and 10, there are not found any significant differences between the responses of the two models - the elastic model (model 1) and the viscoelastic model (model 2). This can be explained as follows: Fig.4 shows that the acceleration versus time curve may be approximated by a sine curve of approximmate period 16 m sec, and this suggests that the dominant exitation frequency is approximately $\omega=2\pi/(16\times10^{-3})=392.7$ rad/sec, for which Fig.7 gives the shear modulus very close to the short time modulus G_1. That is, the response of the brain material is dominantly governed by the short time modulus, which has been used in the elastic modelling. The duration of acceleration transient is very short enough to suppress the memory effect in the response of the silicone gel. This suggests that the short time modulus G_1 is one of the input data of critical importance for accurate prediction in the present numerical simulation. The present numerical results may not be appropriate for accurate quantification of deformation. Taking into consideration the fact that the viscoelastic properties used in the analysis, except for the long time modulus, are determined not from test but from conjecture, however, the results may be considered very encouraging in that the overall deformed configuration and the characteristics of response of the brain material which are observed in the experiment are captured well. Some simple test may be combined with numerical simulation to determine the accurate viscoelastic constants, and use of these may bring a substantial improvement in accuracy.

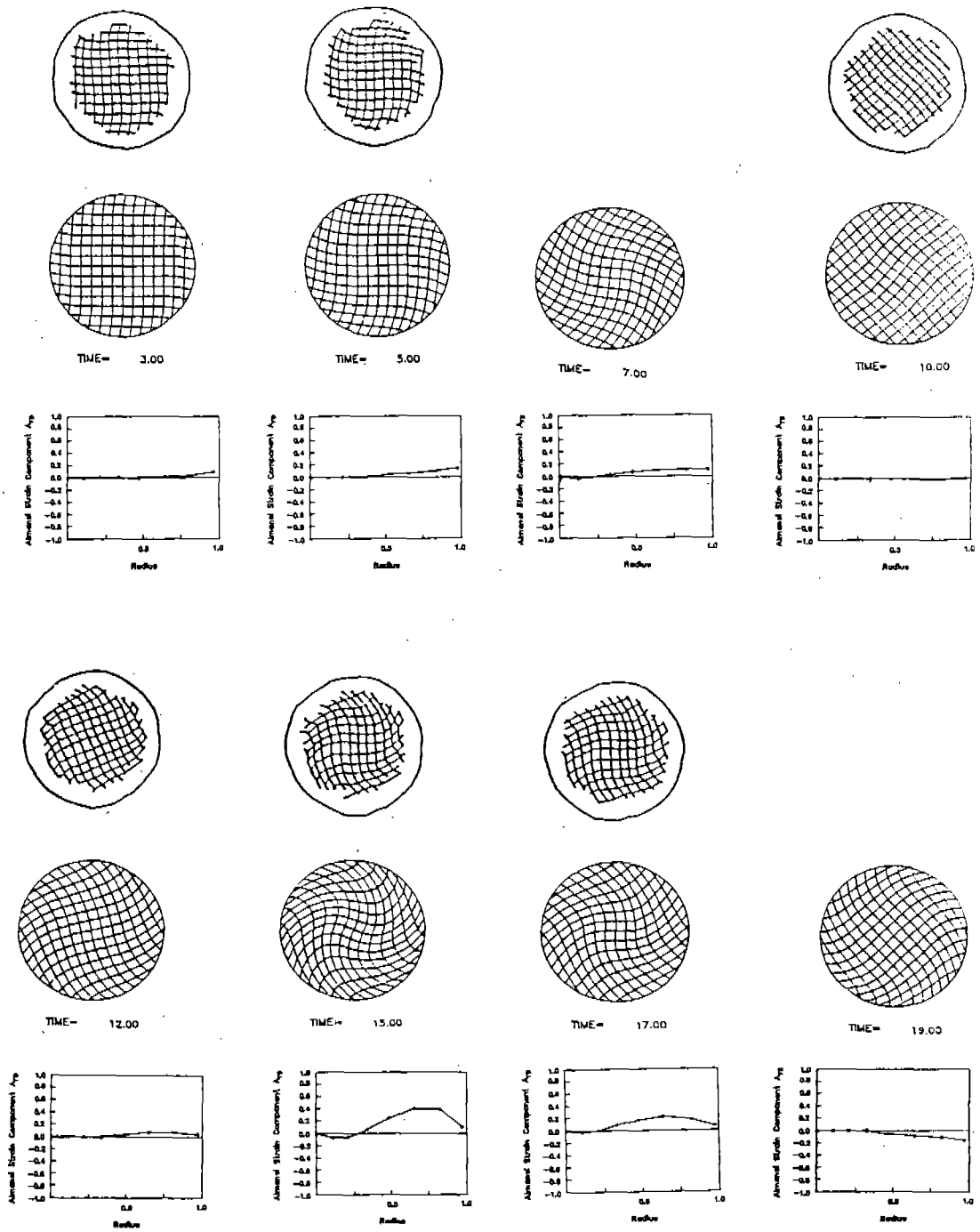

Fig. 9 Deformation profiles and the shear strain for the model 1(top: the test result, middle: the numerical result, bottom:shear strain component of the Almansi strain tensor)

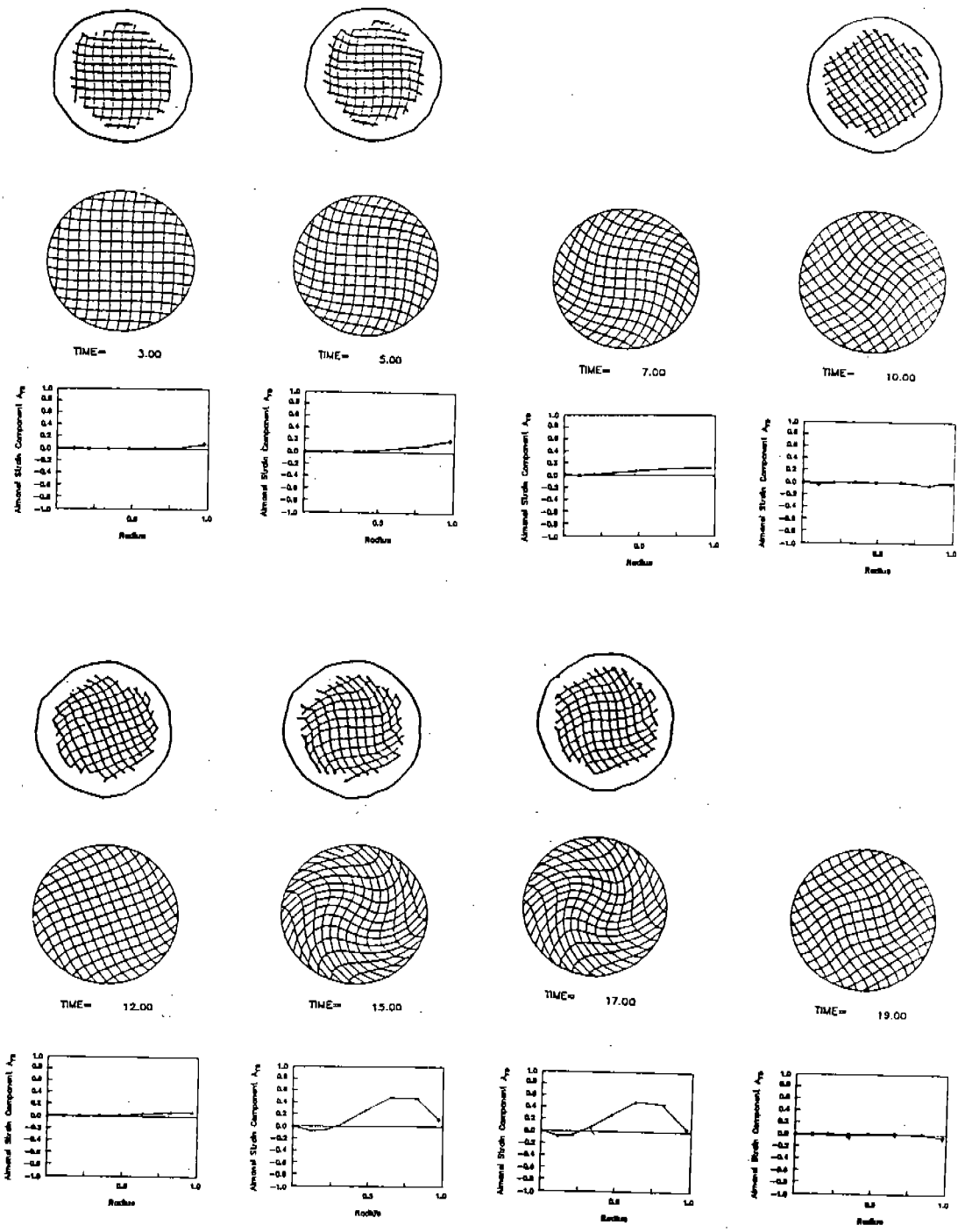

Fig. 10 Deformation profiles profiles and the shear strain for the model 2.

5. Conclusion

With the aid of nonlinear finite element analysis, numerical simulation for the response of a prototype brain material, silicone gel, under rotational transient acceleration has been performed, and a comparison has been made between the results of this simulation and the test results. The deformation profiles and the major characteristics of response of the brain material are in good agreement with the test results. The results of numerical analysis suggest the possibility that the use of more accurate material data, particularly the short time modulus, which may be determined from test for some simple motion in conjunction with numerical simulation, may yield very useful results appropriate for accurate quantification of deformation, so that the numerical simulation may replace the expensive tests.

Acknowledgement

The authors are grateful to Professor S.N. Arluri of Georgia Institute of Technology and Dr. P. Tong of the Department of Transportation for their helpful suggestions during the course of this study. The authors also thank the secretaries of Mechanical Engineering Department, KAIST for their expert assistance in preparing the manuscript.

References

1. Stritch, S.J. "The pathology of brain damage due to blunt head injuries, The late effects of head injury" (edited by Walker, A.E.). C.C. Thomas, Springfield, pp.501-526, 1969.
2. Ommaya, A.K. and Hirch, A.E. "Tolerance for cerebral concussion from head impact and whiplash in primates," J. Biomechanics 4, pp.13-21, 1971.
3. Engine, A.E. and Wang, H.C. "A mathematical model to determine viscoelastic behaviour of in vivo primate brain," J. Biomechanics 3, pp.283-296, 1970.
4. Wang, H.C. and Wineman, A.S. "A mathematical model for the determination of viscoelastic behaviour of brain in vivo-I oscillatory response," J. of Biomechanics 5, pp.571-580, 1972.
5. Lung, C. (1975) "A model for brain deformation due to rotation of skull," J. of Biomechanics 8, pp.263-274.
6. Merchant, H.C. and Crispino, A.J. (1974) "A dynamic analysis of an elastic model of the human head," J. of Biomechanics 7, pp.295-301, 1974.
7. Akkas, N. (1975) "Dynamic analysis of a fluid-filled spherical sandwich shell-A model of the human head", J. of Biomechanics 8, pp.275-284, 1975.
8. Misra, J.C. and Chakravarty "A study on rotational brain injury," J. Biomechanics 17, pp.459-464, 1984.
9. Thibault, L.E., Margulies, S.S., and Gennarelli, T.A., "The temporal and spatial response of a brain model in inertial loading," 31-st stapp car crash conference, pp.267-272, 1987.
10. Thibault, L.E., Department of Transportation Contract Report DTAN-22-82-C-07187, 1982.
11. Malvern, L.E., Introduction to the mechanics of a continuous medium, Prentice-Hall., 1969.
12. Key, S.W. (1974) "A finite element procedure for the large deformation dynamic response of axisymmetric solids," Comp. Meth. App. Mech. Engr., 4, pp.195-217.
13. Simo, J.C. and Pister, K.S., "Remarks on rate constitutive equations for finite deformation problems: computational implications", Comp. Meth. Appl. Mech.

Engr., 46, pp.201-215, 1984.

14. Simo, J.C., "On the dynamics of flexible beams under large overall motions-the plane case: part II," J. Appl. Mech., 53, pp.855-863,

Appendix

Equations (2.a) and (3) read for $t=t^{N+1}$

$$\bar{\underset{\sim}{\sigma}}'^{N+1} = 2\int_0^{t^{N+1}} G_2\,\underset{\sim}{D}'d\tau + 2(G_1-G_2)\int_0^{t^{N+1}} e^{-\alpha(t^{N+1}-\tau)}\,\underset{\sim}{D}'(\tau)d\tau \qquad (A-1)$$

Introducing the relation (17.b), we may recast the above into the following approximate form involving $\underset{\sim}{\sigma}'^{N}$ and $\Delta\underset{\sim}{\varepsilon}'$

$$\bar{\underset{\sim}{\sigma}}'^{N+1} = \bar{\underset{\sim}{\sigma}}'^{N} + 2\{G_2+(G_1-G_2)(1-e^{-\alpha\Delta t})/(\alpha\Delta t)\}\Delta\bar{\underset{\sim}{\varepsilon}} + 2(G_1-G_2)(e^{-\alpha\Delta t}-1)\int_0^{t^N} e^{-\alpha(t^N-\tau)}\underset{\sim}{D}'d\tau \qquad (A-2)$$

Neglecting the 2-nd term and rotating this relation back to the current configuration, we obtain the incremental stress-strain relation in terms of $\Delta\underset{\sim}{\sigma}'^{GR}$ and $\Delta\underset{\sim}{\varepsilon}'$

$$\Delta\underset{\sim}{\sigma}'^{GR} \cong 2\{G_2-(G_1-G_2)(1-e^{-\alpha\Delta t})(\alpha\Delta t)\}\,\Delta\underset{\sim}{\varepsilon}' \qquad (A-3)$$

This relation is combined with the incremetal form for the volumetric deformation, equation (2.b), to yield the complete incremental relation. In the "collapsed representation", this can be written as

$$\begin{pmatrix}\Delta\sigma_{11}^{GR}\\ \Delta\sigma_{22}^{GR}\\ \Delta\sigma_{33}^{GR}\\ \Delta\sigma_{12}^{GR}\\ \Delta\sigma_{23}^{GR}\\ \Delta\sigma_{31}^{GR}\end{pmatrix} \cong \begin{pmatrix} k+\frac{2}{3}A & k-\frac{1}{3}A & k-\frac{1}{3}A & 0 & 0 & 0\\ & k+\frac{2}{3}A & k-\frac{1}{3}A & 0 & 0 & 0\\ & & k+\frac{2}{3}A & 0 & 0 & 0\\ & \text{Symmetric} & & \frac{1}{2}A & 0 & 0\\ & & & & \frac{1}{2}A & 0\\ & & & & & \frac{1}{2}A\end{pmatrix} \begin{pmatrix}\Delta\varepsilon_{11}\\ \Delta\varepsilon_{22}\\ \Delta\varepsilon_{33}\\ 2\Delta\varepsilon_{12}\\ 2\Delta\varepsilon_{23}\\ 2\Delta\varepsilon_{13}\end{pmatrix}$$

where $A = 2G_2 + 2(G_1-G_2)\,(1-e^{-\alpha\Delta t})/(\alpha\Delta t)$